



## Antitubercular drugs for an old target: GSK693 as a promising InhA direct inhibitor



María Martínez-Hoyos<sup>a</sup>, Esther Perez-Herran<sup>a</sup>, Gulcin Gulten<sup>b</sup>, Lourdes Encinas<sup>a</sup>, Daniel Álvarez-Gómez<sup>a</sup>, Emilio Alvarez<sup>a</sup>, Santiago Ferrer-Bazaga<sup>a</sup>, Adolfo García-Pérez<sup>a</sup>, Fátima Ortega<sup>a</sup>, Iñigo Angulo-Barturen<sup>a</sup>, Joaquin Rullas-Trincado<sup>a</sup>, Delia Blanco Ruano<sup>a</sup>, Pedro Torres<sup>a</sup>, Pablo Castañeda<sup>a</sup>, Sophie Huss<sup>a</sup>, Raquel Fernández Menéndez<sup>a</sup>, Silvia González del Valle<sup>a</sup>, Lluís Ballell<sup>a</sup>, David Barros<sup>a</sup>, Sundip Modha<sup>c</sup>, Neeraj Dhar<sup>d</sup>, François Signorino-Gelo<sup>c</sup>, John D. McKinney<sup>c</sup>, Jose Francisco García-Bustos<sup>a</sup>, Jose Luis Lavandera<sup>a</sup>, James C. Sacchettini<sup>b</sup>, M. Soledad Jimenez<sup>e</sup>, Nuria Martín-Casabona<sup>f</sup>, Julia Castro-Pichel<sup>a</sup>, Alfonso Mendoza-Losana<sup>a,\*</sup>

<sup>a</sup> Diseases of the Developing World, GlaxoSmithKline, Severo Ochoa 2, 28760 Tres Cantos, Madrid, Spain

<sup>b</sup> Department of Biochemistry and Biophysics, Texas A&M University, College Station, TX 77843, USA

<sup>c</sup> Target and Pathway Validation, Molecular Discovery Research, GlaxoSmithKline, Stevenage, Herts, UK

<sup>d</sup> School of Life Sciences, Swiss Federal Institute of Technology in Lausanne (EPFL), Lausanne 1015, Switzerland

<sup>e</sup> ISCIII, Crta. Majadahonda-Pozuelo Km 2, Majadahonda 28220, Madrid

<sup>f</sup> Department of Microbiology Vall d'Hebron Hospital, Autonomous University Barcelona, Barcelona, Spain

### ARTICLE INFO

#### Article history:

Received 4 February 2016

Received in revised form 29 April 2016

Accepted 3 May 2016

Available online 8 May 2016

#### Keywords:

Tuberculosis

Antibiotic

InhA

Bactericidal

Drug discovery

Single-cell imaging

Catalase

### ABSTRACT

Despite being one of the first antitubercular agents identified, isoniazid (INH) is still the most prescribed drug for prophylaxis and tuberculosis (TB) treatment and, together with rifampicin, the pillars of current chemotherapy. A high percentage of isoniazid resistance is linked to mutations in the pro-drug activating enzyme KatG, so the discovery of direct inhibitors (DI) of the enoyl-ACP reductase (InhA) has been pursued by many groups leading to the identification of different enzyme inhibitors, active against *Mycobacterium tuberculosis* (*Mtb*), but with poor physicochemical properties to be considered as preclinical candidates. Here, we present a series of InhA DI active against multidrug (MDR) and extensively (XDR) drug-resistant clinical isolates as well as in TB murine models when orally dosed that can be a promising foundation for a future treatment.

© 2016 The Authors. Published by Elsevier B.V. This is an open access article under the CC BY-NC-ND license (<http://creativecommons.org/licenses/by-nc-nd/4.0/>).

### 1. Introduction

Although most of the drugs for tuberculosis were discovered >50 years ago, TB accounts for about 1.4 million deaths every year (Zumla et al., 2013). The majority of the TB cases are treatable with the current long and complex regimen of drugs, although the lack of adherence due to adverse effect is not unusual, leading to suboptimal responses and rising incidences of M(X)DR cases worldwide. In the last 40 years, only two new drugs have been approved for the treatment of MDR-TB under specific conditions: bedaquiline and delamanid (Andries et al., 2005; Thakare et al., 2015). Thus, there is a critical need for the development of drugs with shorter, simpler regimens as

well as novel mechanisms of action that can be used for treatment of drug-resistant forms of the disease.

Both target-based (Makarov et al., 2009) and phenotypic screening (Ballell et al., 2013; Lechartier et al., 2014; Mak et al., 2012; Pethe et al., 2010) approaches have been employed for the identification of anti-tubercular drug leads. While a limited but significant number of examples exist for the latter (Abrahams et al., 2012; Makarov et al., 2009; Remuinan et al., 2013), target-based approaches have encountered very limited success as previously demonstrated in the antibacterial field (Abrahams et al., 2012; Payne et al., 2007). Rather than invalidating the approach per se, this situation highlights the disconnection between concepts like genetic validation of target essentiality and the amenability of that target for drug discovery. A deeper understanding of system biology and the mechanisms underlying antibiotic killing are important for the discovery of new antimicrobial therapies through target-based approaches. Additionally, for reasons that are not always obvious,

\* Corresponding author at: GlaxoSmithKline, Severo Ochoa 2, 28760 Tres Cantos, Madrid, Spain.

E-mail address: [alfonso.x.mendoza@gsk.com](mailto:alfonso.x.mendoza@gsk.com) (A. Mendoza-Losana).

some targets are clearly more chemically tractable than others. For example, protein and cell wall bio-synthesis and DNA gyrase have delivered multiple classes of published leads and marketed drugs, whereas there are no known inhibitors for many other essential gene products, despite a long history of antibacterial research (Kohanski et al., 2010). In the antitubercular field, only a very limited number of targets such as InhA, RpoB, DNA Gyrase, ATP synthase, and DprE1 have been shown to be behind the action of potent bactericidal drugs or promising leads.

Isoniazid is a frontline anti-TB drug targeting InhA and is an essential component of TB treatment regimen. Despite the seemingly simple structure of INH, its mode of action has remained elusive for many years (Vilcheze and Jacobs, 2007). INH penetrates the tubercle bacilli by passive diffusion and is activated by the bacterial *anti*-oxidant enzyme KatG to a range of reactive species and isonicotinic acid. Relevant reactive species form adducts with nicotinamide adenine dinucleotide (NAD), which are able to interfere with NAD-utilizing enzymes, primarily the enoyl-ACP reductase encoded by the *inhA* gene, leading to the blockage of mycolic acid synthesis and delivering the lethal blow to *M. tuberculosis*. The dependency on KatG activation for INH-mediated killing is also the source of the main clinical weakness associated with the use of INH, as between 40% and 95% of INH-resistant MTB clinical isolates have mutations in *katG*, leading to decreased activation of INH to its active form (Hazbon et al., 2006; Seifert et al., 2015). While mutations are also detected in clinical isolates in the *inhA* promoter region, these can be successfully treated in most instances by increasing the dose of isoniazid.

Different classes of direct InhA inhibitors have been identified previously using high-throughput screening, Encoded Library Technology, and *in silico* design strategies (Lu et al., 2010; Manjunatha et al., 2015; Pan and Tonge, 2012; Shirude et al., 2013; Sink et al., 2015; Vilcheze et al., 2011; Encinas et al., 2014). Additionally, natural product pyridomycin has been found to operate via InhA inhibition (Hartkoorn et al., 2012; Lu et al., 2010). Most of these tended to show a lack of correlation between enzymatic inhibition and whole-cell activity, have moderate potencies, narrow selectivity windows or poor absorption, distribution, metabolism, and excretion (ADME) properties, making them unsuitable for further progression as drug leads.

GlaxoSmithKline (GSK), under the sponsorship of the TB Alliance, has carried out a screen against InhA using the GSK compound collection and has identified the thiadiazole series as the most promising antitubercular family. In this study, we present the novel and selective lead compound and its attractive antitubercular properties.

## 2. Materials and methods

The human biological samples were sourced ethically and their research use was according to the terms of the informed consent.

All animal studies were ethically reviewed and carried out in accordance with European Directive 2010/63/EU and the GSK Policy on the Care, Welfare and Treatment of Animals.

### 2.1. Compound Synthesis

GSK613 and GSK625 were obtained from commercial sources. GSK693 was synthesized as described in the patent (Castro-Pichel et al., 2012). Optical rotations were measured on a Rudolph AUTOPOL V polarimeter at room temperature using a cell of 0.5 dm. <sup>1</sup>H NMR spectra were recorded on a Bruker DPX 400 MHz NMR spectrometer. Measurements were made at a temperature of 295 K, and are reported in ppm using tetramethylsilane or solvent as an internal standard (DMSO-*d*<sub>6</sub> at 2.50 ppm). The coupling constants (*J*) are given in Hz, and the splitting patterns are designated as follows: s, singlet; bs, broad singlet; d, doublet; and m, multiplet. <sup>13</sup>C NMR spectra were recorded on a Bruker DPX 400 spectrometer at 295 K and are reported in ppm using solvent as an internal standard (DMSO-*d*<sub>6</sub> at 39.5 ppm). Analytical purity was ≥95%, as determined by <sup>1</sup>H-NMR and HPLC analysis. Positive ion mass

spectra were acquired using a QSTAR Elite (AB Sciex Instruments) mass spectrometer, equipped with a turbospray source, over a mass range of 250–700, with a scan time of 1 s. The elemental composition was calculated using Analyst QS 2.0 software.

**(S)-1-(4-methylthiazol-2-yl)-1-(5-((1-(2-methylthiazol-4-yl)methyl)-1H-pyrazol-3-yl)amino)-1,3,4-thiadiazol-2-yl)ethanol (GSK693):**  $[\alpha]_D^{20} = +119$  (*c* = 1, MeOH). <sup>1</sup>H NMR (300 MHz, DMSO-*d*<sub>6</sub>): δ ppm 10.93 (bs, 1H, –NH), 7.75 (d, *J* = 2.20 Hz, 1H), 7.38 (bs, 1H), 7.33 (s, 1H, –OH), 7.28–7.29 (m, 1H), 6.03 (d, *J* = 2.27 Hz, 1H), 5.32 (s, 2H), 2.68 (s, 3H), 2.37 (s, 3H), 2.02 (d, *J* = 7.03 Hz, 3H). <sup>13</sup>C NMR (100 MHz, DMSO-*d*<sub>6</sub>): δ ppm: 17.38, 19.18, 28.77, 51.32, 74.67, 94.29, 115.29, 117.15, 132.43, 148.65, 151.73, 152.42, 156.50, 164.66, 166.28, 175.79. HRMS (*m/z*):  $[M + H]^+$  calcd. For C<sub>16</sub>H<sub>17</sub>N<sub>7</sub>O<sub>3</sub>S<sub>3</sub>, 420.0730; found, 420.0717.

### 2.2. Bacterial strains and culture

*M. tuberculosis* H37Rv, *Mycobacterium smegmatis* mc<sup>2</sup>155 (Snapper et al., 1990), and *Mycobacterium bovis* BCG Pasteur (Institut Pasteur) were grown at 37 °C in Middlebrook 7H9 broth (Difco) supplemented with 0.025% Tween 80 and 10% albumin–dextrose–catalase (ADC) or on Middlebrook 7H10 plates supplemented with 10% oleic acid–albumin–dextrose–catalase (OADC). Cell-free extracts were done in 7H9 (Difco) supplemented with 100 ml of 10× AS solution (5% albumin solution in salt: 10 mg albumin, 1.7 mg NaCl in 200 ml water), 2.5 ml of 10% Tween 80 solution, and 0.1% carbon substrate (acetamide, succinate, or glucose). *Escherichia coli* DH5α was grown in LB broth (LB).

### 2.3. DNA manipulation, plasmids, and transformation

General molecular biology procedures were used as described previously (Green and Sambrook, 2012) or following the manufacturer instructions. *E. coli* DH5α, *M. smegmatis* mc<sup>2</sup>155, and *M. bovis* BCG competent cells were prepared for electroporation as described previously (Goude et al., 2015; Green and Sambrook, 2012).

### 2.4. Enzymatic purification of InhA

The plasmids were transformed into BL21(DE3) *E. coli* cells for protein overexpression. Cells carrying InhA overexpression plasmid were cultured overnight in LB broth media together with 100 μg/ml ampicillin at 37 °C with continuous shaking at 220 rpm. Then a 1% dilution of the inoculum was made (10 ml of the starter culture into 4 × 1 l) in LB broth media with 100 μg/ml ampicillin, and flasks were incubated till the OD<sub>600</sub> reached 0.7. Cells were induced with 0.5 mM IPTG at 30–32 °C for 3 h, harvested and resuspended for lysis in 100 ml total volume of 10% glycerol, 25 mM Tris pH 8.0, and 2 mM DTT (freshly made) at 4 °C. Cells were then sonicated 4 × 15 s at maximum amplitude with 45 s incubation on ice between pulses and finally centrifuged at 30,000 g at 4 °C for 1 h.

The supernatants were loaded on 6-ml Resource Q columns, which were pre-equilibrated with 25 mM Tris–HCl pH 8.5, 2 mM DTT. Fractions (2.5 ml) were collected over 20 column volumes (gradient of 0–200 mM NaCl, 25 mM Tris–HCl pH 8.2, 2 mM DTT). The fractions were run out on an SDS–PAGE gel and stained with Coomassie. The most concentrated ones were selected and pooled to run on a Superdex 16/60 SEC to help decontaminate. The column was equilibrated with 25 mM Tris–HCl pH 8.0, 2 mM DTT, and the pooled fractions were applied to the column at 0.12 ml/min/1 ml fractions were collected in the following buffer: 20 mM Tris–HCl pH 8.0, 2 mM DTT, 0.15 M NaCl. The column was run overnight, the fractions were checked by SDS–PAGE, and activity was verified by enzymatic assay.

## 2.5. *InhA* biochemical assays

The *trans*-2-enoyl-ACP reductase enzyme of *M. tuberculosis* catalyzes the last step in the elongation cycle of the FAS-II pathway and reduces the 2.3 double bond of *trans*-2-enoyl-ACP in a NADH-dependent manner. High-throughput screening (HTS) and led optimization (LO) biochemical assays are based in the oxidation of the cofactor in the presence of dodecenoyl-CoA.

*InhA* inhibition by file compounds in a high-throughput format was assessed using a substrate-induced quenching (SIQ) assay as described previously (Vazquez et al., 2006). Reaction mixtures (3  $\mu$ l) containing 100  $\mu$ M test compound, 150  $\mu$ M dodecenoyl-CoA, 100  $\mu$ M NAD<sup>+</sup>, 30  $\mu$ M NADH, 10 nM resorufin, 0.2% w/v pluronic acid F-127, 10 nM resorufin, 0.01% BSA, 1% DMSO, and 1.25 nM *InhA* in 30 mM PIPES buffer at pH 6.8 were incubated in glass-bottom 1536-well plates for 1 h at 20 °C and 95% relative humidity. Plates were then read in a confocal microscope (4-Channel Reader, Evotec Technologies) using 1D-FIDA settings with beamscanner, Nd:Yag 532 nm excitation with a laser power of 150  $\mu$ W for 200 ms/well. Confocal FLINT data from each screening plate were normalized against control wells containing reaction mixtures in the absence of test compounds (high controls) and in the absence of enzyme (low controls). Assay quality was monitored for each plate using the Z' factor (Zhang et al., 1999) and the inhibition observed in additional control wells containing a known inhibitor at its IC<sub>50</sub>. In order to identify and discard signal quenchers, each plate was pre-read before addition of enzyme.

Enzymatic activity to support LO phase was measured fluorimetrically by following NADH oxidation at  $\lambda_{exc}$  = 340 nm and  $\lambda_{em}$  = 480 nm, using 50  $\mu$ M NADH and 50  $\mu$ M 2-*trans*-dodecenoyl-CoA (DDCoA) as substrates. Dose–response experiments to determine IC<sub>50</sub> were performed using 5 nM *InhA*, percentage of remaining enzymatic activity (%AR) at different compound concentrations were calculated with the next formula [%AR = 100\*((sample – control 2) / (control 1 – control 2))] where sample is the enzymatic activity for each compound concentration, control 1 is enzyme activity in absence of any compound, and control 2 is NADH oxidation in absence of enzyme; IC<sub>50</sub> was calculated fitting %AR to a 2-parameter equation [%AR = 100 / (1 + (compound conc / IC<sub>50</sub>)<sup>s</sup>)], where s is a slope factor; IC<sub>50</sub> was calculated using GraFit 5.0.12 software (Eritacus Software Ltd.). All reactions were run in 30 mM PIPES buffer, pH 6.8, at 25 °C.

## 2.6. Crystallization, data collection, and processing

The *InhA*:GSK625 complex was crystallized using the hanging drop method; 0.2 mM *InhA*, 2 mM NAD<sup>+</sup>, and 2 mM GSK625 that was dissolved in 100% DMSO were incubated at room temperature for ~20 min and screened against sparse-matrix crystallization conditions. The crystals were obtained in 1.1 M sodium malonate, 0.1 M HEPES pH 7.0, and 0.5% (v/v) Jeffamine ED-2001 pH 7.0.

The diffraction data were collected at home source, at 120 K under cryoprotection by a Rigaku Raxis detector coupled to an X-ray generator with a rotating copper anode ( $\lambda$  = 1.541 Å). Data were processed by Denzo and Scalepack software packages (Otwinowski and Minor, 1997). Crystals of the *InhA*:NAD<sup>+</sup>:GSK625 complex belonged to the P2<sub>1</sub>2<sub>1</sub>2<sub>1</sub> space group with four molecules in the ASU. *InhA*:GSK625 structure was solved by molecular replacement using the PDB entry 1ENY as a search model. The structure was built by Coot and further refined by Phenix (Adams et al., 2010) yielding a final model with  $R_{work}$  = 20% and  $R_{free}$  = 23%. Data processing statistics are given in Supplementary Table 1. PDB ID 1BVR.

## 2.7. Cloning and overexpression of *InhA*

Double digestion with *Bgl*II and *Bam*HI liberates *M. smegmatis* and *M. tuberculosis inhA* genes from plasmids pATB15 and pATB14 (Parish et al., 1997), respectively. The 918- and 917-bp fragments were cloned into

pATB45 previously linearized by *Bam*HI digestion. Ligations were performed into *E. coli* DH5 $\alpha$ . The final plasmids were verified by enzymatic fragments analysis and both *inhA* genes were sequenced. Sequencing was carried out with using the dideoxy chain-termination procedure and reagents from Applied Biosystems (dRhodamine Terminator Cycle Sequencing Ready Reaction kit) in an ABI Prism 310 automated DNA sequencer (Applied Biosystems). The electroporation of *M. smegmatis* mc<sup>2</sup>155 and *M. bovis* BCG was carried out according to the method of (Snapper et al., 1990), and transformants were selected on Middlebrook 7H10 plates supplemented with 10% OADC and hygromycin 50  $\mu$ g/ml. Transformant verifications were made by colony PCR by using the PuRe Taq Ready-To-Go PCR Beads kit (GE Healthcare Life Sciences) with the primers colony PCR 1 and 2. The sequences of the primers were as follows: Primer colony 1, 5'-AATCCAAAGTTCAAACGAGGGG-3'; Primer colony 2, 5'-CCACCACCCGATAAGAGAAAGG-3'. The following thermocycler parameters were used: an initial denaturation step of 5 min at 94 °C, followed by 35 cycles of 30 s at 94 °C, 30 s at 62 °C and 3 min at 72 °C, and ending with a final elongation step of 10 min at 72 °C.

Protein expression levels were followed by SDS–PAGE. Cell-free extracts were obtained from *M. smegmatis* mc<sup>2</sup>155 and *M. bovis* BCG by growing them in 500 ml Middlebrook 7H9 broth with 0.025% Tween 80 and 10% ADC (1 l conical flask) to log phase (OD 600 nm  $\approx$  0.6) harvested by centrifugation (5000 rpm for 5 min) and resuspended in 5 ml sterile distilled water. A quantity 0.5 ml of *M. smegmatis* mc<sup>2</sup>155 cells was used to inoculate 250 conical flasks containing 100 ml minimal medium with either acetamide 1%, succinate 0.1%, or succinate 0.1% plus acetamide 1%. A quantity 0.5 ml of *M. bovis* BCG cells was used to inoculate 250 ml conical flasks containing 100 ml minimal medium with either acetate 0.1%, acetate 0.1% plus acetamide 1%, ADC 10% or ADC 10% plus acetamide 1%. Cultures were incubated at 37 °C and harvested after 24 h (*M. smegmatis* mc<sup>2</sup>155) or 7 days (*M. bovis* BCG).

Cell-free extracts were prepared from both cultures using the Mini-BeadBeater (Biospec Products): 50 ml bacterial cells, resuspended in 1 ml 50 mM HEPES/KOH pH 7.5, 10 mM MgCl<sub>2</sub>, 60 mM NH<sub>4</sub>Cl, 10% (v/v) glycerol, and 5 mM 2-mercaptoethanol, were added to 0.5 ml of 0.1 mm sterile glass beads and shaken for 1 min three times, incubating the samples on ice 1 min between pulses. The supernatant was recovered after centrifugation. Cell-free extracts were analyzed by SDS–PAGE (Laemmli, 1970); protein concentration was determined using the BCA protein assay (Pierce).

## 2.8. Isolation and characterization of *M. tuberculosis* H37Rv GSK625-resistant mutants

GSK625-resistant *M. tuberculosis* H37Rv mutants were isolated by plating 10<sup>8</sup> CFU on Middlebrook 7H10 plates supplemented with 10% OADC containing the compound at 20  $\mu$ M (20xMIC). After 4 weeks of incubation at 37 °C, colonies were identified and purified through several passages in inhibitor-containing plates. Single colonies were used to amplify and sequence *inhA* alleles. DNAs of the 17 resistant mutants were extracted from liquid cultures grown in Middlebrook 7H9 broth supplemented with 0.025% Tween 80 and 10% ADC. One milliliter of culture was centrifuged, and the pellet was resuspended in 500  $\mu$ l of distilled water and incubated at 90 °C for 1 h and then filtrated by using 0.22  $\mu$ m filters. Five microliters of the supernatant was used as a source of genomic DNA for amplification of the *inhA* gene. PCRs of the entire gene were performed for each mutant by using the PuRe Taq Ready-To-Go PCR Beads kit (GE Healthcare Life Sciences). A 988-bp region was amplified with the primers Forward (5'-CAGCTTCCTGGCTTCCGAG-3') and Reverse (5'-TAACGTTCTCCAGGAACGG-3'), and PCR conditions were an initial denaturation step of 5 min at 94 °C, followed by 40 cycles of 30 s at 94 °C, 30 s at 62 °C, and 3 min at 72 °C and ending with a final elongation step of 10 min 72 °C. PCR products were purified and sequenced using the dRhodamine Terminator Cycle Sequencing Ready Reaction kit (Applied



Biosystems) in an ABI Prism 310 automated DNA sequencer (Applied Biosystems).

### 2.9. Complementation experiments

The whole *fabG1-inhA-hemH* operon from wild-type H37Rv and mutants carrying the four mutant alleles (M103V, G96V, M103I, and M103T) were cloned in the shuttle vector pSUM36 (Ainsa et al., 1996). *M. tuberculosis* H37Rv was transformed with the five plasmids and transformants were selected using kanamycin and verified by colony PCR using the PuRe Taq Ready-To-Go PCR Beads kit (GE Healthcare Life Sciences). The sequences of the primers were as follows: pSUM36\_2, 5'-GTTGTGTGGAATTGTGAGCGG-3'; InhArev1, 5'-GAAACGCGATCGACGAGTCCG-3'. The following thermocycler parameters were used: an initial denaturation step of 9 min at 94 °C, followed by 40 cycles of 30 s at 94 °C, 30 s at 64 °C, and 3 min at 72 °C and ending with a final elongation step of 10 min 72 °C. Positive transformants were used MIC determination.

### 2.10. MIC determination against *Mycobacteria*

The antitubercular activity against extracellular of intracellular *Mycobacterium* strains was performed as previously described (Blanco-Ruano et al., 2015).

### 2.11. MIC against clinical strains

The BACTEC MGIT 960 System (Becton Dickinson) was used to MIC determination in clinical isolates (Institute Carlos III and Hospital Val d'Hebron) following the manufacturer instructions.

### 2.12. General antimicrobial activity assay

Whole-cell antimicrobial activity was determined by broth microdilution using the Clinical and Laboratory Standards Institute (CLSI) recommended procedure, Document M7-A7 (Wikler, 2009). Compounds have been evaluated against a panel of Gram-positive and Gram-negative organisms, including *Enterococcus faecium*, *Enterococcus faecalis*, *Haemophilus influenzae*, *Moraxella catarrhalis*, *Streptococcus pneumoniae*, *E. coli*, and *Streptococcus pyogenes*. The MIC was determined as the lowest concentration of compound producing a reduction in the observed fluorescence higher than 80%.

### 2.13. hERG inhibition determination and cell cytotoxicity assays

hERG Qpatch assay was described by Vasilyev et al. (2006). Cell cytotoxicity assays was described by Crouch et al. (1993).

### 2.14. Kinetic solubility assay

Here, 5 ml of 10 mM DMSO stock solution was diluted to 100 ml with phosphate-buffered saline, pH 7.4, equilibrated for 1 h at room temperature, and filtered through Millipore Multiscreen HTS-PCF filter plates (MSSL BPC). The eluent was quantified by suitably calibrated flow injection CLND.

### 2.15. Cytochrome P450 (CYP450)

The P450 inhibition profile of the InhA inhibitors was determined as previously described in reference (Kajbaf et al., 2011).

### 2.16. Tolerability studies

For tolerability studies C57BL/6 female mice of 18–20 g weight were used ( $n = 6$  mice). Drugs were administered as 1% methyl-cellulose suspensions. The up-and-down method of experimentation is an

adaptive procedure for conducting dose–response experiments having yes/no end point. Animals are dosed one at a time at the best estimate MNL. The dose for each successive animal is adjusted up or down, depending on the outcome of the previous animal. After reaching the reversal of the initial direction (the point where a decreasing dose pattern requires an increase due a tested animal's survival or an increasing dose pattern results in a decrease due to lethality), four additional animals are dosed using the same up and down dose pattern. The maximal no lethal dose is calculated using the maximum likelihood algorithm. If any animal died or acute clinical signs were noted, the up-and-down procedure was carried out based on toxicological signs (functional observational battery). According to the up-and-down statistical procedure based on if, two dose levels were determined; a dose that caused adverse clinical signs to 5% of animals (SD05) and a higher one that causes signs of toxicity at 95% of animals (SD95). Functional observational battery (FOB) and bodyweight gain were recorded and the animals were killed 24 h and 48 h after treatment and blood was sampled by intra-cardiac puncture for clinical chemistry and hematology analysis in He-Li tubes. Necropsy was carried out and the major organs were weighed and preserved in formalin.

### 2.17. Microsomal fraction stability experimental procedure

Pooled mouse and human liver microsomes were purchased from Xenotech. Microsomes (final protein concentration 0.5 mg/ml, 5 mM MgCl<sub>2</sub>), and test compound (final substrate concentration 0.5 μM; final DMSO concentration 0.5%) in 0.1 M phosphate buffer pH 7.4 was pre-incubated at 37 °C prior to the addition of NADPH (final concentration 1 mM) to initiate the reaction. The final incubation volume was 600 μl. Control samples were included for each compound tested where 0.1 M phosphate buffer pH 7.4 was added instead of NADPH (minus NADPH). Midazolam was included as control in every experiment. Each compound was incubated for 30 min and samples (90 μl) were taken at 0, 5, 10, 20, and 30 min. The minus NADPH control was sampled at 0 and 30 min only. The reactions were stopped by the addition of 200 μl of acetonitrile:methanol (3:1) containing an internal standard, followed by centrifugation at 3700 rpm for 15 min at 4 °C to precipitate the protein. Quantitative analysis was performed using specific LC-MS/MS conditions. Data analysis: from a plot of ln peak area ratio (compound peak area/internal standard peak area) against time, the gradient of the line was determined. Subsequently, half-life and intrinsic clearance were calculated using the equations below:

Elimination rate constant( $k$ ) = (-gradient)

$$\text{Half life}(t_{1/2})(\text{min}) = \frac{0.693}{k}$$

$$\text{Intrinsic clearance}(CL_{int})(\text{ml}/\text{min}/\text{g tissue}) = \frac{V \times 0.693}{t_{1/2}}$$

where  $V$  = incubation volume ml/g microsomal protein and constant used for mg microsomal protein/g liver is 52.5.

### 2.18. Killing kinetics assay

Bacteria were grown at 37 °C in 7H9 broth, 10% ADC, and 0.025% Tyloxapol to mid-exponential phase and then diluted in 10 ml fresh Middlebrook 7H9 to an  $5 \times 10^5$  CFUs/ml. Incubation was continued after the addition of compounds at 20xMIC. At specified time points, aliquots of cultures were withdrawn, serially diluted in 7H9 broth 0.025% Tyloxapol and plated on solid culture medium. Plates were then incubated at 37 °C and CFU were counted after 3 to 4 weeks.

### 2.19. Time-lapse imaging

Time-lapse imaging of the GFP expressing MTB strain growing in the custom-made microfluidic device was carried out as described before (Wakamoto et al., 2013). Briefly, cells were grown in 7H9 medium at 37 °C to mid-log phase and were seeded into the microfluidic device for imaging. Images were acquired at 1 h intervals on the phase and FITC (Excitation 490/20; Emission 528/38) channels using a DeltaVision personalDV imaging system (Applied Precision) equipped with a 100× objective (Olympus UPLFL 100× PH, 1.3 NA) and a CoolSnap HQ2 camera. Medium and compound were replenished every 24 h. As an end-point assay, 1.0 µg/ml propidium iodide was added to the flow medium for 24 h to stain cells with permeabilized cell envelopes and imaging done on the red channel (Excitation 555/28; Emission 617/73).

Analysis of the time-lapse image stacks was carried out using ImageJ v 1.47a (<http://rsb.info.nih.gov/ij/>). The survival curves depicted in Fig. 4 were generated by tracking cell division and lysis events over the course of the experiment using the “Cell Counter” plugin of ImageJ. Cytolysis was scored visually by abrupt loss of GFP fluorescence and abrupt decrease in phase intensity. Statistic analysis and fitting of data was performed using Prism (GraphPad).

### 2.20. Mice

Specific Pathogen-free 6- to 8-week-old female C57BL/6j mice (18–20 g) are obtained from Harlan (Harlan Interfauna Iberica, Spain). The experiments were performed at AAALAC-accredited GlaxoSmithKline Laboratory Animal Science animal facilities in Tres Cantos (Madrid, Spain). The mice were kept in air-conditioned facilities with fifteen air changes per hour. Room temperature and relative humidity were 22 ± 3 °C and 40–70%, respectively. The mice were accommodated in groups of up to five individuals in Tecniplast® type IV cages with autoclaved dust free corn cob bedding (Panlab, Barcelona, Spain). The mice were maintained under a 12-h light/dark period. Autoclaved tap water and  $\gamma$ -irradiated pelleted diet were provided ad libitum.

### 2.21. Pharmacokinetic studies

Pharmacokinetic studies were performed in C57BL/6j female mice of 18–20 g weight ( $n = 4$  mice per time point). Experimental compounds were administered by intravenous route at 0.5 (GSK613 and GSK625) or 4 mg/kg (GSK693) single dose at a volume of 10 ml/kg and by oral gavage at 50 (GSK613 AND 625), 100, 150, or 300 mg/kg single doses (GSK693) at a volume of 20 ml/kg. All mice received treatment in the fed state. Compounds were administered as solution in 1% DMSO, 7.5% PEG400, and 20% Encapsine in saline for intravenous route and as 1% methyl-cellulose suspension for oral route. Whole blood was the compartment chosen for the establishment of compound concentrations: blood samples were taken by cardiac puncture for each mouse (euthanized by CO<sub>2</sub>) at 5, 15, and 30 min, 1, 1.5, 2, 3, 4, and 8 h ( $n = 4$  mice per time point) for intravenous route and at 15, 30, and 45 min, 1, 1.5, 2, 3, 4, and 8 h ( $n = 4$  mice per time point) for oral route. LC-MS was used as the analytical method of choice for the establishment of compound concentration in blood with a sensitivity of LLQ = 1–5 ng/ml in 25 µl blood. The non-compartmental data analysis (NCA) was performed with WinNonlin 5.2 (Pharsight, Certara L.P), and supplementary analysis was performed with GraphPad Prism 5 (GraphPad Software, Inc).

### 2.22. In vivo acute efficacy assessment

The experimental design has been previously described (Rullas et al., 2010). In brief, mice were intratracheally infected with 100,000 CFU/mouse (*M. tuberculosis* H37Rv). Products were administered for 8 consecutive days starting 1 day after infection. Lungs were harvested 24 h after the last administration. For the chronic assay, mice were infected with 100 CFU/mouse, and the products were administered daily

(7 days a week) for 8 consecutive weeks starting 6 weeks after infection. All lung lobes were aseptically removed 24 h after the last administration, homogenized, and frozen. Homogenates were plated in 10% OADC-7H11 medium for 14 days at 37 °C. Homogenates from compound treated mice were incubated for 18 days at 37 °C in plates supplemented with 0.4% (wt, vol) activated charcoal (Sigma Aldrich) to prevent the effect of product carryover. Moxifloxacin (Sequoia Research Products Ltd.) was prepared as solution in 20% Captisol(R)/water).

### 2.23. In vivo chronic efficacy assessment

Specific pathogen-free, 8- to 10-week-old female C57BL/6j mice were purchased from Harlan Laboratories and were allowed to acclimate for 1 week. In brief, mice were intratracheally with 100 CFU/mouse and the products administered daily (7 days a week) for 4 or 8 consecutive weeks starting 6 weeks after infection. Lungs were harvested 24 h after the last administration. All lung lobes were aseptically removed, homogenized, and frozen. Homogenates were plated in 10% OADC-7H11 medium supplemented with activated charcoal (0.4%) for 18 days at 37 °C. The positive control of isoniazid was assayed at 25 mg/kg, in distilled water.

## 3. Results

### 3.1. Biochemical, physicochemical, and ADME characterization of hits GSK613 and GSK625

Several screening campaigns were run against InhA yielding an overall hit rate of 0.63% after quencher removal. The campaign covered a total of 1.9 million compounds unearthing GSK613 and GSK625 as the most attractive representative structures of the thiadiazole series. Both compounds exhibited a single-digit nanomolar activity in the enzyme assay and micromolar in the whole-cell assay and showed selective antibacterial activity against *M. tuberculosis*. The physicochemical properties and preliminary ADMET profile were completed (Table 1) and used to drive medicinal chemistry efforts.

*N*-(1-(2-chloro-6-fluorobenzyl)-1H-pyrazol-3-yl)-5-(1-(3-methyl-1H-pyrazol-1-yl)ethyl)-1,3,4-thiadiazol-2-amine (GSK613) was progressed to enzymatic mode of action studies to discard non-specific enzyme inhibition. GSK613 is a selective (inactive against human FAS), reversible inhibitor in addition to time, enzyme, and solvent independent. Steady-state competition experiments have shown that the hit competes with the fatty acid substrate for binding to the enzyme but is uncompetitive with NADH, consistent with inhibitors binding to a pre-formed enzyme:NADH complex (see Supplementary Fig. 1, Supplementary Table 2).

### 3.2. Use of *InhA* overexpressor strain to confirmation whole-cell mode of action

Two *Mycobacterium smegmatis* mc<sup>2</sup>155 and *Mycobacterium bovis* BCG strains expressing increased levels of *InhA* protein from *M. smegmatis* and *M. tuberculosis* were constructed in order to identify inhibitors whose whole-cell activity is mediated mainly or solely by inhibition of *InhA* (see Supplementary Fig. 2). A reproducible shift in the minimum inhibitory concentration (MIC) values higher than or equal to 4-fold in strains overexpressing the target was considered as indicative that antitubercular activity is mainly mediated by *InhA* inhibition. Thiadiazoles GSK625 and GSK613 met this criterion.

### 3.3. Structure of the *InhA*:GSK625 complex

Crystal structures were obtained for *InhA* in complex with NAD<sup>+</sup> and the thiadiazole compound GSK625 at 2.9 Å resolution (see Supplementary Table 1) (PDB ID 5JFO). The electronic density observed was used for identifying the main scaffold and its disposition and interactions within the active site (Fig. 1).

**Table 1**

Structure of hit compounds GSK613 and GSK625. Compounds were assessed for activity against purified InhA, *M. tuberculosis* H37Rv, a panel of Gram-positive and Gram negative bacteria, and HepG2 mammalian cells, ClogP, and DMPK parameters (*in vitro* and *in vivo* clearance, volume of distribution at steady state (Vss), half-life ( $t_{1/2}$ ), Tmax, Cmax, and dose normalized exposure (DNAUC) in mice).

	GSK613	GSK625
InhA IC50	7 nM	2 nM
<i>Mtb</i> MIC	≤1 μM	1 μM
Antibacterial panel	≥64 μg/ml	≥64 μg/ml
MW	403.9	417.9
ClogP	3.75	4.05
Art. Memb. Permeability	3.4 × 10 <sup>-5</sup> cm/s	5.4 × 10 <sup>-5</sup> cm/s
Solubility CLND HepG2	10 μM	9 μM
cytotoxicity Tox 50	>100 μM	>100 μM
<i>In vitro</i> Cli mouse	11.9 ml/min/g	14.9 ml/min/g
<i>In vitro</i> Cli human	2.9 ml/min/g	2.8 ml/min/g
<i>In vivo</i> pharmacokinetic studies in mice		
<i>In vivo</i> Cl (0.5 mg/kg iv)	156.7 ml/min/kg	119.9 ml/min/kg
<i>In vivo</i> Vss (0.5 mg/kg iv)	2.5 L/kg	1.5 L/kg
<i>In vivo</i> t <sub>1/2</sub> (0.5 mg/kg iv)	0.3 h	0.2 h
<i>In vivo</i> Tmax (50 mg/kg po)	0.75 h	1 h
<i>In vivo</i> Cmax (50 mg/kg po)	94.3 ng/ml	2383 ng/ml
DNAUC (ng·h/ml per mg/kg)	5	123

GSK625 was observed bound to the hydrophobic substrate-binding pocket of InhA, which was surrounded by residues M199, L207, I215, M103, F149, Y158, A198, and I202 (residue numbering as in reference (Lu et al., 2010; Rozwarski et al., 1999)). We were able to crystallize the enzyme:inhibitor complex only in the presence of the cofactor

NAD(H), in agreement with the uncompetitive character of these inhibitors relative to NADH (Fig. 1). When the structures of the InhA:GSK625 and that of the InhA:NAD<sup>+</sup>:C16-fatty acyl substrate analog complex (Rozwarski et al., 1999) were compared, it was observed that the aromatic pyrazole ring of the inhibitor occupied the same pocket as the thioester and the *trans* double bond of the C16-substrate analog, in close proximity to NAD<sup>+</sup>, which is in agreement with the competitive behavior of these inhibitors relative to the DDCoA substrate.

The pyrazole ring interacted with NAD<sup>+</sup> via π-π stacking (4 Å). In addition, the pyrazole nitrogen H-bonded to the 2'-hydroxyl of the ribose moiety in the cofactor (3.3 Å). The other key interactions identified were the direct H-bonding between (i) the nitrogen of the thiadiazole ring and the amide NH of Met98 and (ii) the nitrogen linking the pyrazole and the thiadiazole rings and the carbonyl oxygen of Met98 (2.9 and 2.5 Å, respectively). Hydrophobic and van der Waals interactions between the inhibitor and the side chains of the active site residues Met161, Phe97, Leu207, Met199, Met103, Gly 104, Met98, Ala198, Gly96, Phe149, Tyr158, and Ile202 dominated the ligand-protein interactions. The halide substituted aryl ring of GSK625 interacted with the main chain Met199, and Gly104, through its halogen atoms, which increased the potency remarkably compared to the analogs without the aryl moiety. Noticeably, the catalytic residue Tyr158 did not make any H-bonds with the inhibitor and participated in ligand binding through van der Waals interactions only (3.9 Å). Thus, GSK625 is a representative of a class of inhibitors which does not need this conserved network of interaction with Tyr158 for potency. Furthermore, in the InhA:NAD<sup>+</sup>:GSK625 complex, the side chain of Phe149 adopted the identical position as in InhA:NAD(H) structure.

#### 3.4. The thiadiazole series is bactericidal

To test if these inhibitors shared the fast killing mode of action of INH, we determined the *in vitro* killing rates of GSK625 at 20xMIC in growth medium inoculated with approximately 10<sup>6</sup> bacteria, during 7 days (Fig. 2). After the first 2 days of incubation, the thiadiazole behaved similarly to INH, killing >99% of the initial bacteria. Due to the high frequency of spontaneous resistance to INH, the number of bacteria increases after 4 days of culture in presence of this drug, but not so in cultures treated with GSK625, where the number of colony forming units kept decreasing down to the detection limit.

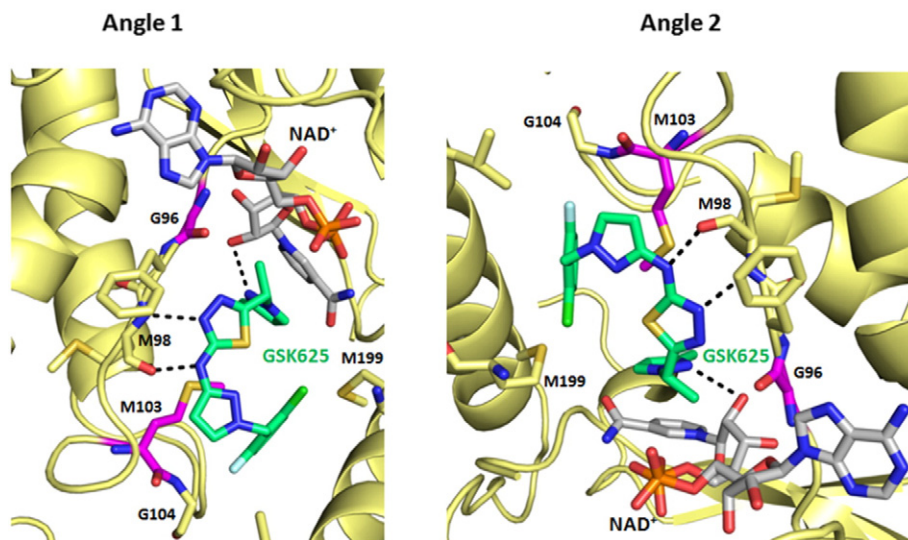


**Fig. 1.** X-Ray structure of InhA-GSK625 complex: Binding mode of GSK625 to the InhA active site. GSK625 (green) interacted with NAD<sup>+</sup> (gray) and M98 via H-bonds (shown as black dashed lines), with G96, F97, M98, M103, F149, M161, I202, G104, M199, and L207 through hydrophobic and van der Waals interactions. The two residues involved in resistance, G96 and M103, are colored in magenta. Atom coloring is oxygen red, nitrogen blue, sulfur yellow, chlorine green, and fluoride light blue.



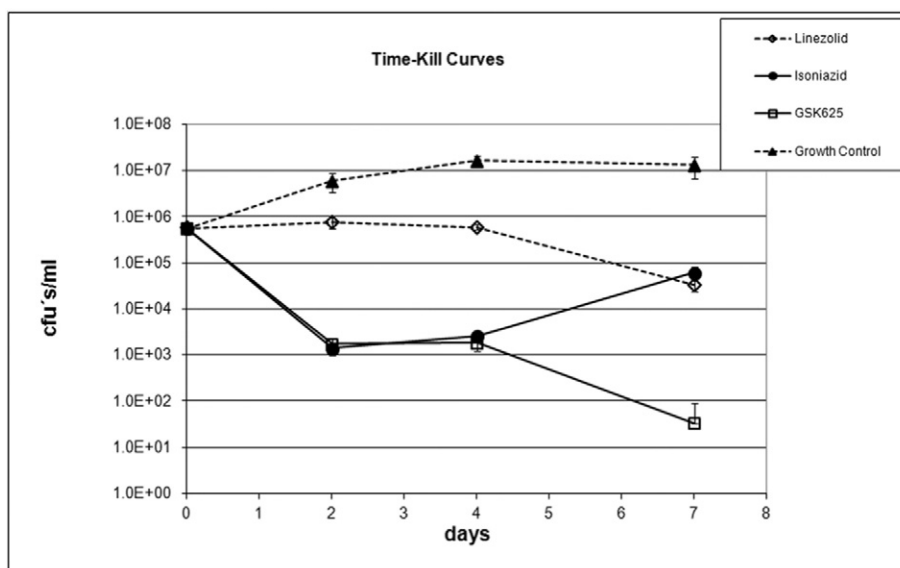


Fig. 2. Killing curve of GSK625. Killing rates of *M. tuberculosis*, exposed to 20xMIC of GSK625, INH, and linezolid.

### 3.5. GSK625 generates resistant mutants at lower frequency than INH and mutations map in the *InhA* active site

The *in vitro* rate of spontaneous resistance for GSK625 at 20xMIC was  $3.7 \times 10^{-8}$  mutants/CFU, very similar to the frequency obtained with rifampicin and three orders of magnitude lower than that for isoniazid (Zhang and Yew, 2009). This rate is consistent with the presence of a single defined target. GSK625-resistant mutants exhibited a shift in MIC value by at least one order of magnitude and display no cross-resistance with other antitubercular compounds such as INH and rifampicin. Since the compounds bind to the enzyme competitively with DDCoA, it could be expected that mutations in the substrate-binding site could affect the interaction of the thiadiazoles, while leaving isoniazid (INH) and ethionamide (ETH) activity unaffected. The *inhA* alleles from single colonies of the seventeen mutants were amplified and sequenced. Four different point mutations were found in the coding regions from all mutants, producing a single amino acid change at either of two positions: Gly96 or Met103. These two amino acids map to the active site of the enzyme (see Supplementary Table 3) and have not been reported to be involved in resistance to *InhA* neither for isoniazid or ethionamide.

In order to link the point mutations in *inhA* to the resistant phenotype, the enoyl-ACP-reductase from the wild type and the four different point mutants were over-expressed and purified as untagged protein in *E. coli*. All the mutated enzymes behaved similarly than the wild type and a very good correlation between enzymatic  $IC_{50}$  for inhibition with GSK625 and the MIC values of the source strains was observed (see Supplementary Table 4). For the whole-cell analysis, the complete *inhA* operon (*fabG1-inhA-hemZ*) from the wild-type H37Rv strain and from the resistant mutants were cloned in a multicopy plasmid and transformed in fast growing *M. smegmatis* mc<sup>2</sup>155 and in *M. tuberculosis* H37Rv. In all cases, the genetic transformation of the mutant operons conferred resistance to thiadiazoles well above that obtained by expressing the wild type version from the multicopy plasmid (see Supplementary Fig. 3).

### 3.6. Activity of GSK625 against sensitive and M(X)DR *M. tuberculosis* clinical isolates

*InhA* inhibitors, such as INH and ETH, have been in use for decades and resistant MTB strains have emerged without identifiable mutations in *inhA* or in any other studied gene (Sandgren et al., 2009). It was

therefore relevant to test a variety of clinical drug-resistant isolates for the possibility of pre-existing cross-resistance to the thiadiazole class. Two thiadiazole compounds were tested in a first instance against a group of INH-resistant clinical isolates with characterized mutations, either in *katG* (the most frequent resistant class) or in nucleotide position 15 upstream of the transcription start site for *inhA* (*InhA* overexpressor) (Sandgren et al., 2009; Vilcheze and Jacobs, 2007). The compounds retained full activity against the first group of mutants, while a moderate shift (4–8 times) in MIC was observed against the group of strains overexpressing *InhA*, as described above for laboratory constructs (Table 2).

GSK625 has been tested against recent clinical isolates of *M. tuberculosis* at two different TB reference centers (National Institute of Health Carlos III, Madrid and the Supranational Reference Laboratory of the Hospital Vall d'Hebron, Barcelona), and two observations were noteworthy. The first one was that the MIC<sub>90</sub> obtained with 100 recently isolated MTB strains is 3  $\mu$ M, showing that the thiadiazole sensitivity of our laboratory H37Rv strain is representative for the majority of MTB strains isolated in Spain, which are therefore sensitive to the compound (see Supplementary Table 5). The second was that GSK625 is active against most resistant isolates present in the sample, with MIC values similar to that of laboratory strain H37Rv independently of the resistance profile of the clinical strains (see Supplementary Table 6).

### 3.7. Lead optimization summary, lead profile

Despite the interesting *in vitro* antitubercular profile stated above, the initial hits were affected by a number of compound development liabilities such as physicochemical properties and DMPK profile. Further medicinal chemistry efforts (details to be reported elsewhere) were

Table 2  
Activity of thiadiazoles (GSK613, GSK625) and controls (kanamycin, *InhA* and ETH) against *M. bovis* BCG overexpressing *InhA*.

Compound/strain	Wild type	– 15 C/T <i>inhA</i> katG S315T							
		H37Rv	C11	C12	C13	C14	C15	C16	C17
GSK625	MIC ( $\mu$ M)	1	8	16	8	2	1	2	2
	Ratio	1	8	16	8	2	1	2	2
	MIC ( $\mu$ g/ml)	0.5	3.125	1.6	1.6	50	50	25	200
INH	MIC ( $\mu$ g/ml)	0.5	3.125	1.6	1.6	50	50	25	200
	Ratio	1	6	3	3	100	100	50	400

hence dedicated to the identification of optimized compounds. These efforts led to the identification of the chiral compound GSK693 as a promising lead (Table 3).

GSK693 retained the enzymatic activity of previous GSK613 and GSK625 hits. Additionally, GSK693 displayed equal potency against the *M. tuberculosis* H37Rv inside and outside of macrophages (0.2  $\mu$ M). This was accompanied by a good CYP 3A4 inhibition profile. Early safety assessment was carried out, across different enzymatic assays. GSK693 did not show any sign of cytotoxicity and no hERG potassium channel inhibition (Vasilyev et al., 2006), suggesting a low risk for general toxicity and cardiotoxicity. Genotoxicity alert was discarded with a full Ames test (McCann et al., 1975). The breakthrough in the developability was obtained with the decreased lipophilicity, the enhanced solubility, and the reduced metabolic liabilities whilst simultaneously achieving good mouse pharmacokinetic exposure levels after a single oral administration at different doses (see Supplementary Table 7). Cross-resistance experiments with previously isolated mutants proved that the observed TB activity for the lead compound was target related (data not shown). Additional biological studies were carried out to confirm and gain further insight into the mode of action of GSK693.

### 3.8. Single-cell analysis of effect of GSK693 on *M. tuberculosis*

To confirm that the synthesized derivatives retain the antitubercular properties of the original hits, we evaluated the bactericidal activity of GSK693 against MTB at the single-cell level by culturing the bacteria in microfluidic devices and observing their behavior by time-lapse microscopy. MTB expressing GFP was grown in a microfluidic device for 6 days until they formed small microcolonies. The bacteria were then exposed to 5  $\mu$ M (2.1  $\mu$ g/ml–25xMIC) GSK693 for 10 days, followed by washout of the drug for 7 days. Exposure to GSK693 induced a rapid growth arrest of individual MTB cells quite similar to the response of MTB when exposed to INH. Interestingly, while in case of INH, the cells continued to divide without elongation for several hours and started to lyse after a lag of several days, in case of GSK693, the cell lysis was more rapid without any significant lag period (see Supplementary Fig. 4). While the total fraction of cells undergoing lysis was comparable between GSK693 (53  $\pm$  20%  $N$  = 32 microcolonies) and INH

(42  $\pm$  15%,  $N$  = 41 microcolonies), the bacteriolysis induced by GSK693 was significantly more rapid than INH ( $P$  = 0.011, log-rank Mantel–Cox test). In both cases, after exposure to INH or GSK693, the rate of killing was maintained even after washout of the drug, indicative of strong post-antibiotic effect or long-term inhibition of the target by the compounds. In order to identify cells that did not lyse visibly but whose cell wall was potentially compromised, we stained the remaining intact cells with propidium iodide (PI) as an end point assay. About 22% of the cells still intact after GSK693 exposure were found to be PI-positive and remarkably the remaining 78% of the cells were still able to exclude PI. None of the intact bacteria exhibited regrowth after washout of the drug, possibly suggestive again of long-term target inhibition or possible pushing of the surviving bacterial population into a non-replicative senescent state.

### 3.9. Confirmation of *KatG*-independent activity of GSK693

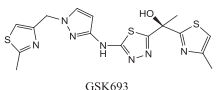
As shown previously in Table 2, thiazazole compounds exhibited no change in MIC against INH-resistant clinical isolates carrying mutations in *katG*. However, since MIC is more of an assay of bacteriostatic activity, we decided to confirm the *katG*-independent bactericidal activity of GSK693. We compared the killing efficacy of INH vs GSK693 against a panel of three strains differing in the level of *KatG* expression—(i) a wild-type *M. tuberculosis* with the native *katG* locus; (ii) a *katG*-null mutant of *M. tuberculosis*, deficient in catalase activity (Ng et al., 2004); and (iii) a *katG*-overexpressing strain of *M. tuberculosis* that carries a second copy of MTB *katG* at the *atTB* locus. These strains were exposed to 3.6  $\mu$ M (0.5  $\mu$ g/ml) INH or 5  $\mu$ M of GSK693 for 4 days and the fraction of bacteria surviving antibiotic treatment determined by plating. As expected, against INH, the *katG*-null mutant was resistant, and the *katG*-overexpressing strain was more sensitive compared to the wild-type strain (Fig. 3). Encouragingly and consistent with our previous observations, the *katG*-null mutant strain was killed equally well as the wild-type strain by GSK693. This further reinforces the *katG*-independent nature of bactericidal activity of GSK693.

### 3.10. *In vivo* efficacy of GSK693 in the acute and chronic TB murine infection models

Given its desirable and balanced profile, GSK693 fulfilled our requirements to be progressed to tolerability and *in vivo* efficacy studies in both acute and chronic TB murine infection models. The maximal no lethal dose (MNL) in mice was found to be higher than 1000 mg/kg. Subsequently, the oral efficacy of GSK693 was evaluated in an acute murine model as previously described (Rullas et al., 2010) at doses of 30, 100, and 300 mg/K u.i.d. for 7 days, using moxifloxacin as

**Table 3**

Structure and properties of optimized lead GSK693. The lead was assessed for activity against *M. tuberculosis* H37Rv both intra and extracellularly, physicochemical, and ADMET properties.

 GSK693		
Physchem properties	MW	419.6
	ClogP	0.71
	Art. Memb. Permeability	1.9 · 10 <sup>-5</sup> cm/s
	Solubility CLND	413 $\mu$ M
Activity profile	InhA IC <sub>50</sub>	7 nM
	<i>Mtb</i> MIC	0.2 $\mu$ M
	<i>Mtb</i> intracell MIC	0.2 $\mu$ M
Cytochrome P450 profile	CYP 3A4 IC <sub>50</sub> VR	> 50.1 $\mu$ M
	CYP 3A4 IC <sub>50</sub> VG	25.1 $\mu$ M
	HepG2 Cytotoxicity Tox 50	>50 $\mu$ M
Cytotoxicity profile	Cell Health (Memb.; Nucleus; Mitoch. )	>199.5 $\mu$ M
	Ames test	Negative
Cardiovascular profile	Qpatch IC <sub>50</sub>	>50 $\mu$ M
In vitro metabolic stability	Cli mouse	2.1 ml/min/g
	Cli human	0.2 ml/min/g
	Cl (4 mg/kg iv)	83 ml/min/kg
	Vss (4 mg/kg iv)	2.58 L/kg
In vivo pharmacokinetic study in mice	t1/2 (4 mg/kg iv)	0.94 h
	Tmax (100 mg/kg po)	0.42 h
	Cmax (100 mg/kg po)	37,271 ng/ml
	DNAUC	935.8 ng · h/ml per mg/kg

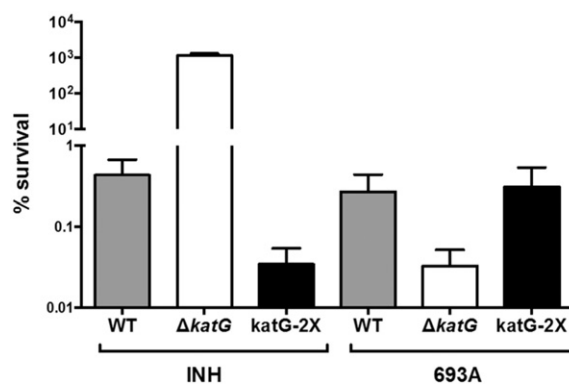


**Fig. 3.** GSK693 exhibits *KatG*-independent bactericidal activity. This plot depicts the percent survival of wild-type *M. tuberculosis* (WT); a *katG*-null catalase-deficient mutant strain of *M. tuberculosis* ( $\Delta katG$ ); and a *katG*-overexpressing strain of *M. tuberculosis* (*katG*-2x) after exposure to 3.6  $\mu$ M INH or 5  $\mu$ M GSK693 for a period of 4 days. Data shown represents the Mean + SE of three independent replicates.



a positive control at 30 mg/kg. The compound showed a clear dose/response pharmacological effect with this dose range (Fig. 4a). In mice treated with 100 mg/kg, the bacterial load was reduced 4 log<sub>10</sub> colony forming units (CFU) per lung, matching the reduction obtained with 30 mg/kg of moxifloxacin.

The important proof-of-concept *in vivo* efficacy was obtained by GSK693 in the acute murine TB model. GSK693 was further evaluated in an established model of TB infection at a dose of 300 mg/kg as suspension in 1% methylcellulose. After a 2-month treatment of chronically infected mice, GSK693 (300 mg/kg) and isoniazid (25 mg/kg), showed a clear efficacy (Fig. 4b), and the differences observed between both groups were not statistically significant.

The bacterial load reduction in both acute and chronic murine models with GSK693 at 300 mg/kg is virtually the same than the one observed with isoniazid at the human equivalent dose.

#### 4. Discussion

Isoniazid (INH) is together with rifampicin the corner stone of the TB treatment. It has been administrated to >40 million people saving millions of lives. Its outstanding cidal effect rapidly blocks bacterial spread and significantly improves patient's conditions after a few weeks of treatment.

On the basis of INH mode of action, it has been proposed that direct inhibitors of the enoyl-ACP-reductase of Mtb can retain the outstanding antitubercular profile of INH overcoming most of the issues associated with the drug, such as drug resistance and toxicological effects. Additionally, compounds inhibiting InhA without requiring activation by

KatG could be active under anaerobic conditions (Vilcheze et al., 2011), where catalase-mediated activation is suppressed by the lack of oxygen (Karakousis et al., 2008).

Following the above-mentioned rationale, a biochemical assay based on NADH consumption in the presence of docecenoyl-CoA by purified InhA enzyme has allowed the identification of different direct inhibitors of Mtb enoyl-ACP reductase. All the compounds showing IC<sub>50</sub> values in the micromolar range were clustered and tested for antitubercular activity against wild-type and InhA overexpressor strains to identify five chemical series of bona-fide inhibitors (whole-cell activity clearly linked to enzymatic inhibition).

Enzymatic and whole-cell activities will provide the desired efficacy at an acceptable dose, but a drug also needs to have the right physicochemical properties to increase the probability of success (Hann and Keseru, 2012). The drug-like chemical properties of the selected InhA inhibitors were evaluated to select thiadiazole series as the family with the best balance between potency and physicochemical properties.

GSK613 and GSK625 are the most attractive representative compounds of the thiadiazole series. Both exhibited a single-digit nanomolar activity in the enzyme assay and micromolar in the whole-cell assay and showed a selective antibacterial activity against *M. tuberculosis*. The series does not require KatG activation and retain the antitubercular activity against sensitive, MDR, and XDR clinical isolates.

The *in vitro* frequency of spontaneous resistance is three orders of magnitude better than the one obtained for isoniazid. The four different point mutations identified conferring resistance were found in *inhA* coding region, producing a single amino acid change at either of two positions: Gly96 or Met103. These two amino acids map to the active site of the enzyme and have not been reported to be involved in resistance to InhA neither for isoniazid or ethionamide.

Like other InhA direct inhibitors, thiadiazoles bind to the enzyme-NADH complex, but in contrast to previously crystallized InhA inhibitors such as pyrrolidine carboxamides (He et al., 2006), Genzyme10850, and triclosan (Kuo et al., 2003), thiadiazoles do not establish any direct interaction with Tyr158, and unlike the isoniazid-NADH adduct, GSK625 does not cause the flipping of the Phe149 side chain and thus there is no interaction with the isonicotinic acid binding pocket.

Recently, it was proposed that high-affinity slow binding inhibition of InhA is related to the ordering of the substrate-binding loop, brought about by the long residence time of inhibitors on the enzyme (Lu et al., 2010). Importantly, in all of the co-crystal structures with thiadiazoles, the substrate-binding loop (residues 197–226) was ordered and well resolved in the crystal structure, as previously seen with high-affinity slow onset FabI inhibitor structures, implying that the compounds may also be slow, tight binding inhibitors, which generally enhances the *in vivo* activity and increases their potential as antitubercular drugs.

The medicinal chemistry efforts have been focused on the improvement of the physicochemical properties and DMK profile. GSK693 retains all the antitubercular properties shown by the initial hits accompanied by a good cytochrome P450 profile, lack of cardiovascular liabilities, non-mutagenic, reduced lipophilicity, and good solubility which translate to good oral bioavailability. Dosed orally as a 1% methyl-cellulose suspension, the compound has shown a clear antitubercular activity in the acute and chronic mouse models at free compound exposures similar to those obtained with isoniazid.

#### 5. Conclusion

Standard antitubercular treatment consists of a combination of four compounds (isoniazid, rifampicin, ethambutol, and pyrazinamide) during 2 months that eliminate all the fast growing bacteria and 4 additional months of isoniazid and rifampicin that complete patient cure.

The treatment is long, complex, and has important adverse effects, so the lack of adherence is not unusual, leading to suboptimal responses (failure and relapse), emergence of resistance, and continuous spread of the disease. The presence of rapidly bactericidal compounds like

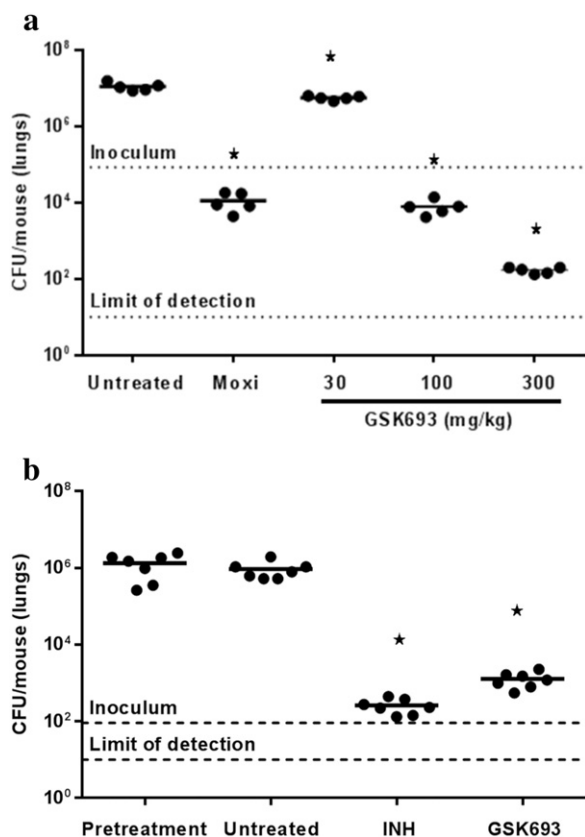


**Fig. 4.** (a) Dose–response studies in acute murine model of TB efficacy. Log CFU in mice after oral treatment with different doses of GSK693 (30, 100, and 300 mg/kg) and moxifloxacin at 30 mg/kg. Treatment in all groups resulted in a significant clearance of bacilli compared with the controls ( $P < 0.001$ ). (b) Efficacy response of GSK693 in chronic, established murine model of TB infection. Log CFU in mice after oral treatment with GSK693 at 300 mg/kg and INH at 25 mg/kg. Treatment in both groups resulted in a significant clearance of bacilli compared with the controls ( $P < 0.001$ ).

isoniazid as part of the combination has a high impact in blocking transmission and improving the health of infected people.

We have demonstrated that a direct inhibitor on InhA can retain the outstanding profile of isoniazid and considering the DMPK parameters of both compounds the antitubercular effect is achieved at similar exposures of free drug proving our initial hypothesis and overcoming resistances mediated by KatG. GSK693 has demonstrated *in vivo* efficacy comparable to the marketed drug isoniazid without being a pro-drug, thus overcoming most of INH associated liabilities. Besides, its improved property profile should translate into a safer treatment. Overall, this achievement opens the door to the development of a direct inhibitor of the enoyl-ACP reductase (InhA) as an attractive drug candidate for the therapy of Tuberculosis.

### Author contributions

MMH and EPH have performed all the target-engagement experiments (whole-cell mode of action tools development, mutant selection, and characterization). DB performed MIC studies. SM has expressed and purified InhA mutated proteins for biochemical experiments. DAG has performed the biochemical experiments to support SAR of thiazidazole series and mutant characterization. EA managed the screening campaign that identified the new series of inhibitors. MSJ and NMC determined the activity of the new compounds against sensitive and resistant clinical isolates. PT and PC performed *in vitro* and *in vivo* cytotoxicity studies respectively. AGP, FA, and SH performed the PK bioanalysis under the supervision of SFB. JR performed *in vivo* studies directed by IAB. JLL performed molecular modeling and data analysis. GG expressed and purified protein for structural experiments, obtaining and analyzing crystallographic data under the supervision of JCS. JCP directed chemistry. LE, SGV, RFM, and LLB synthesized compounds and participate in data analysis and compound designed. ND, FSC, and JDM generated single-cell microscopy data. DB organized and coordinated ORCHID consortium. JFG, EPH, and AML organized and planned biology studies. AML wrote the manuscript with input from the co-authors.

### In memoriam statement

In memoriam of Emilio Alvarez, an example of professionalism, comradeship, and inspiration. His scientific knowledge, advice, and wisdom will be greatly missed.

### Funding sources

The research leading to these results has received funding from GlaxoSmithKline R&D the Global Alliance for TB Drug Development, and from the European Union's 7th framework program (FP7-2007-2013) under the Orchid grant agreement no. 261378.

### Conflict of interest

All the authors confirm the absence of any conflict of interest.

### Appendix A. Supplementary data

Supplementary data to this article can be found online at <http://dx.doi.org/10.1016/j.ebiom.2016.05.006>.

### References

Abrahams, K.A., Cox, J.A., Spivey, V.L., Loman, N.J., Pallen, M.J., Constantinidou, C., Fernandez, R., Alemparte, C., Remuinan, M.J., Barros, D., Ballell, L., Besra, G.S., 2012. Identification of novel imidazo[1,2-a]pyridine inhibitors targeting *M. tuberculosis* QcrB. *PLoS One* 7, e52951.

Adams, P.D., Afonine, P.V., Bunkoczi, G., Chen, V.B., Davis, I.W., Echols, N., Headd, J.J., Hung, L.W., Kapral, G.J., Grosse-Kunstleve, R.W., McCoy, A.J., Moriarty, N.W., Oeffner, R., Read, R.J., Richardson, D.C., Richardson, J.S., Terwilliger, T.C., Zwart, P.H., 2010.

PHENIX: a comprehensive python-based system for macromolecular structure solution. *Acta Crystallogr. D Biol. Crystallogr.* 66, 213–221.

Ainsa, J.A., Martin, C., Cabeza, M., De la Cruz, F., Mendiola, M.V., 1996. Construction of a family of *Mycobacterium/Escherichia coli* shuttle vectors derived from pAL5000 and pACYC184: their use for cloning an antibiotic-resistance gene from *Mycobacterium fortuitum*. *Gene* 176, 23–26.

Andries, K., Verhasselt, P., Guillemont, J., Gohlmann, H.W., Neefs, J.M., Winkler, H., Van, G.J., Timmerman, P., Zhu, M., Lee, E., Williams, P., de, C.D., Huitric, E., Hoffner, S., Cambau, E., Truffot-Pernot, C., Lounis, N., Jarlier, V., 2005. A diarylquinoline drug active on the ATP synthase of *Mycobacterium tuberculosis*. *Science* 307, 223–227.

Ballell, L., Bates, R.H., Young, R.J., Alvarez-Gomez, D., Alvarez-Ruiz, E., Barroso, V., Blanco, D., Crespo, B., Escribano, J., Gonzalez, R., Lozano, S., Huss, S., Santos-Villarejo, A., Martin-Plaza, J.J., Mendoza, A., Rebollo-Lopez, M.J., Remuinan-Blanco, M., Lavandera, J.L., Perez-Herran, E., Gamo-Benito, F.J., Garcia-Bustos, J.F., Barros, D., Castro, J.P., Cammack, N., 2013. Fueling open-source drug discovery: 177 small-molecule leads against tuberculosis. *ChemMedChem* 8, 313–321.

Blanco-Ruano, D., Roberts, D.M., Gonzalez-Del-Rio, R., Alvarez, D., Rebollo, M.J., Perez-Herran, E., Mendoza, A., 2015. Antimicrobial susceptibility testing for *Mycobacterium* sp. In: Parish, T., Roberts, D.M. (Eds.), *Mycobacteria Protocols*. Springer, Hatfield, Hertfordshire, AL10 9AB, UK, pp. 257–268.

Castro-Pichel, J., Fernandez-Menendez, R., Fernandez-Velando, E. P., Gonzalez-Del-Valle, S., and Mallo-Rubio, A. 2012 3-Amino-pyrazole derivatives useful against tuberculosis. PCT/EP2011/067705[WO 2012/049161 A1]. 19–4–2012. Ref Type: Patent.

Crouch, S.P., Kozlowski, R., Slater, K.J., Fletcher, J., 1993. The use of ATP bioluminescence as a measure of cell proliferation and cytotoxicity. *J. Immunol. Methods* 160, 81–88.

Encinas, L., O'Keefe, H., Neu, M., Remuinan, M.J., Patel, A.M., Guardia, A., Davie, C.P., Perez-Macias, N., Yang, H., Convery, M.A., Messer, J.A., Perez-Herran, E., Centrella, P.A., Alvarez-Gomez, D., Clark, M.A., Huss, S., O'Donovan, G.K., Ortega-Muro, F., McDowell, W., Castaneda, P., Arico-Muendel, C.C., Pajk, S., Rullas, J., Angulo-Barturen, I., Alvarez-Ruiz, E., Mendoza-Losana, A., Ballell, P.L., Castro-Pichel, J., Eviñdar, G., 2014. Encoded library technology as a source of hits for the discovery and lead optimization of a potent and selective class of bactericidal direct inhibitors of *Mycobacterium tuberculosis* InhA. *J. Med. Chem.* 57, 1276–1288.

Goude, R., Roberts, D.M., Parish, T., 2015. Electroporation of *Mycobacteria*. In: Parish, T., Roberts, D.M. (Eds.), *Mycobacteria Protocols*. Springer, Hatfield, Hertfordshire, AL10 9AB, UK, pp. 117–130.

Green, M.R., Sambrook, J., 2012. Molecular cloning: a laboratory manual. Cold Spring Harbor Laboratory Press, Cold Spring Harbor, N.Y.

Hann, M.M., Keseru, G.M., 2012. Finding the sweet spot: the role of nature and nurture in medicinal chemistry. *Nat. Rev. Drug Discov.* 11, 355–365.

Hartkoorn, R.C., Sala, C., Neres, J., Pojer, F., Magnet, S., Mukherjee, R., Uplekar, S., Boy-Rottger, S., Altmann, K.H., Cole, S.T., 2012. Towards a new tuberculosis drug: pyridomycin—nature's isoniazid. *EMBO Mol. Med.* 4, 1032–1042.

Hazbon, M.H., Brimacombe, M., Bobadilla, d.V., Cavatore, M., Guerrero, M.I., Varma-Basil, M., Billman-Jacobe, H., Lavender, C., Fyfe, J., Garcia-Garcia, L., Leon, C.I., Bose, M., Chaves, F., Murray, M., Eisenach, K.D., Sifuentes-Osornio, J., Cave, M.D., Ponce de, L.A., Alland, D., 2006. Population genetics study of isoniazid resistance mutations and evolution of multidrug-resistant *Mycobacterium tuberculosis*. *Antimicrob. Agents Chemother.* 50, 2640–2649.

He, X., Alian, A., Stroud, R., Ortiz de Montellano, P.R., 2006. Pyrrolidine carboxamides as a novel class of inhibitors of enoyl acyl carrier protein reductase from *Mycobacterium tuberculosis*. *J. Med. Chem.* 49, 6308–6323.

Kajbaf, M., Longhi, R., Montanari, D., Vinco, F., Rigo, M., Fontana, S., Read, K.D., 2011. A comparative study of the CYP450 inhibition potential of marketed drugs using two fluorescence based assay platforms routinely used in the pharmaceutical industry. *Drug Metab. Lett.* 5, 30–39.

Karakousis, P.C., Williams, E.P., Bishai, W.R., 2008. Altered expression of isoniazid-regulated genes in drug-treated dormant *Mycobacterium tuberculosis*. *J. Antimicrob. Chemother.* 61, 323–331.

Kohanski, M.A., Dwyer, D.J., Collins, J.J., 2010. How antibiotics kill bacteria: from targets to networks. *Nat. Rev. Microbiol.* 8, 423–435.

Kuo, M.R., Morbidoni, H.R., Alland, D., Sneddon, S.F., Gourlie, B.B., Staveski, M.M., Leonard, M., Gregory, J.S., Janjigian, A.D., Yee, C., Musser, J.M., Kreiswirth, B., Iwamoto, H., Perozzo, R., Jacobs Jr., W.R., Sacchetti, J.C., Fidock, D.A., 2003. Targeting tuberculosis and malaria through inhibition of Enoyl reductase: compound activity and structural data. *J. Biol. Chem.* 278, 20851–20859.

Laemmli, U.K., 1970. Cleavage of structural proteins during the assembly of the head of bacteriophage T4. *Nature* 227, 680–685.

Lechartier, B., Rybniker, J., Zumla, A., Cole, S.T., 2014. Tuberculosis drug discovery in the post-post-genomic era. *EMBO Mol. Med.*

Lu, X.Y., You, Q.D., Chen, Y.D., 2010. Recent progress in the identification and development of InhA direct inhibitors of *Mycobacterium tuberculosis*. *Mini-Rev. Med. Chem.* 10, 181–192.

Mak, P.A., Rao, S.P., Ping, T.M., Lin, X., Chyba, J., Tay, J., Ng, S.H., Tan, B.H., Cherian, J., Duraiswamy, J., Bifani, P., Lim, V., Lee, B.H., Ling, M.N., Beer, D., Thayalan, P., Kuhlen, K., Chatterjee, A., Supek, F., Glynn, R., Zheng, J., Boshoff, H.I., Barry III, C.E., Dick, T., Pethe, K., Camacho, L.R., 2012. A high-throughput screen to identify inhibitors of ATP homeostasis in non-replicating *Mycobacterium tuberculosis*. *ACS Chem. Biol.* 7, 1190–1197.

Makarov, V., Manina, G., Mikusova, K., Mollmann, U., Ryabova, O., Saint-Joanis, B., Dhar, N., Pasca, M.R., Buroni, S., Lucarelli, A.P., Milano, A., De, R.E., Belanova, M., Bobovska, A., Dianiskova, P., Kordulakova, J., Sala, C., Fullam, E., Schneider, P., McKinney, J.D., Brodin, P., Christophe, T., Waddell, S., Butcher, P., Albrethsen, J., Rosenkrands, I., Brosch, R., Nandi, V., Bharath, S., Gaonkar, S., Shandil, R.K., Balasubramanian, V., Balganes, T., Tyagi, S., Grosset, J., Riccardi, G., Cole, S.T., 2009. Benzothiazinones kill *Mycobacterium tuberculosis* by blocking arabinan synthesis. *Science* 324, 801–804.

- Manjunatha, U.H., SP, S.R., Kondreddi, R.R., Noble, C.G., Camacho, L.R., Tan, B.H., Ng, S.H., Ng, P.S., Ma, N.L., Lakshminarayana, S.B., Herve, M., Barnes, S.W., Yu, W., Kuhen, K., Blasco, F., Beer, D., Walker, J.R., Tonge, P.J., Glynn, R., Smith, P.W., Diagona, T.T., 2015. Direct inhibitors of InhA are active against *Mycobacterium tuberculosis*. *Sci. Transl. Med.* 7, 269ra3.
- McCann, J., Choi, E., Yamasaki, E., Ames, B.N., 1975. Detection of carcinogens as mutagens in the Salmonella/microsome test: assay of 300 chemicals. *Proc. Natl. Acad. Sci. U. S. A.* 72, 5135–5139.
- Ng, V.H., Cox, J.S., Sousa, A.O., MacMicking, J.D., McKinney, J.D., 2004. Role of KatG catalase-peroxidase in mycobacterial pathogenesis: countering the phagocyte oxidative burst. *Mol. Microbiol.* 52, 1291–1302.
- Otwinowski, Z., Minor, W., 1997. Processing of x-ray diffraction data collected in oscillation mode. In: Carter, J.C.W., Sweet, R.M. (Eds.), *Methods in Enzymology*. Academic Press, New York.
- Pan, P., Tonge, P.J., 2012. Targeting InhA, the FASII enoyl-ACP reductase: SAR studies on novel inhibitor scaffolds. *Curr. Top. Med. Chem.* 12, 672–693.
- Parish, T., Mahenthiralingam, E., Draper, P., Davis, E.O., Colston, M.J., 1997. Regulation of the inducible acetamidase gene of *Mycobacterium smegmatis*. *Microbiology* 143 (Pt 7), 2267–2276.
- Payne, D.J., Gwynn, M.N., Holmes, D.J., Pompliano, D.L., 2007. Drugs for bad bugs: confronting the challenges of antibacterial discovery. *Nat. Rev. Drug Discov.* 6, 29–40.
- Pethe, K., Sequeira, P.C., Agarwalla, S., Rhee, K., Kuhen, K., Phong, W.Y., Patel, V., Beer, D., Walker, J.R., Duraiswamy, J., Jiricek, J., Keller, T.H., Chatterjee, A., Tan, M.P., Ujjini, M., Rao, S.P., Camacho, L., Bifani, P., Mak, P.A., Ma, I., Barnes, S.W., Chen, Z., Plouffe, D., Thayalan, P., Ng, S.H., Au, M., Lee, B.H., Tan, B.H., Ravindran, S., Nanjundappa, M., Lin, X., Goh, A., Lakshminarayana, S.B., Shoen, C., Cynamon, M., Kreiswirth, B., Dartois, V., Peters, E.C., Glynn, R., Brenner, S., Dick, T., 2010. A chemical genetic screen in *Mycobacterium tuberculosis* identifies carbon-source-dependent growth inhibitors devoid of in vivo efficacy. *Nat. Commun.* 1, 57.
- Remuinan, M.J., Perez-Herran, E., Rullas, J., Alemparte, C., Martínez-Hoyos, M., Dow, D.J., Afari, J., Mehta, N., Esquivias, J., Jimenez, E., Ortega-Muro, F., Fraile-Gabaldon, M.T., Spivey, V.L., Loman, N.J., Pallen, M.J., Constantinidou, C., Minick, D.J., Cacho, M., Rebollo-Lopez, M.J., Gonzalez, C., Sousa, V., Angulo-Barturen, I., Mendoza-Losana, A., Barros, D., Besra, G.S., Ballell, L., Cammack, N., 2013. Tetrahydropyrazolo[1,5-a]pyrimidine-3-carboxamide and N-benzyl-6',7'-dihydrospiro[piperidine-4,4'-thieno[3,2-c]pyran] analogues with bactericidal efficacy against *Mycobacterium tuberculosis* targeting MmpL3. *PLoS ONE* 8, e60933.
- Rozwarski, D.A., Vilcheze, C., Sugantino, M., Bittman, R., Sacchettini, J.C., 1999. Crystal structure of the *Mycobacterium tuberculosis* enoyl-ACP reductase, InhA, in complex with NAD<sup>+</sup> and a C16 fatty acyl substrate. *J. Biol. Chem.* 274, 15582–15589.
- Rullas, J., Garcia, J.I., Beltran, M., Cardona, P.J., Caceres, N., Garcia-Bustos, J.F., Angulo-Barturen, I., 2010. Fast standardized therapeutic-efficacy assay for drug discovery against tuberculosis. *Antimicrob. Agents Chemother.* 54, 2262–2264.
- Sandgren, A., Strong, M., Muthukrishnan, P., Weiner, B.K., Church, G.M., Murray, M.B., 2009. Tuberculosis drug resistance mutation database. *PLoS Med.* 6, e2.
- Seifert, M., Catanzaro, D., Catanzaro, A., Rodwell, T.C., 2015. Genetic mutations associated with isoniazid resistance in *Mycobacterium tuberculosis*: a systematic review. *PLoS ONE* 10, e0119628.
- Shirude, P.S., Madhavapeddi, P., Naik, M., Murugan, K., Shinde, V., Nandishaiah, R., Bhat, J., Kumar, A., Hameed, S., Holdgate, G., Davies, G., McMiken, H., Hegde, N., Ambady, A., Venkatraman, J., Panda, M., Bandodkar, B., Sambandamurthy, V.K., Read, J.A., 2013. Methyl-thiazoles: a novel mode of inhibition with the potential to develop novel inhibitors targeting InhA in *Mycobacterium tuberculosis*. *J. Med. Chem.* 56, 8533–8542.
- Sink, R., Sosis, I., Zivec, M., Fernandez-Menendez, R., Turk, S., Pajk, S., Alvarez-Gomez, D., Lopez-Roman, E.M., Gonzales-Cortez, C., Rullas-Triconado, J., Angulo-Barturen, I., Barros, D., Ballell-Pages, L., Young, R.J., Encinas, L., Gobec, S., 2015. Design, synthesis, and evaluation of new thiazole-based direct inhibitors of enoyl acyl carrier protein reductase (InhA) for the treatment of tuberculosis. *J. Med. Chem.* 58, 613–624.
- Snapper, S.B., Melton, R.E., Mustafa, S., Kieser, T., Jacobs Jr., W.R., 1990. Isolation and characterization of efficient plasmid transformation mutants of *Mycobacterium smegmatis*. *Mol. Microbiol.* 4, 1911–1919.
- Thakare, R., Soni, I., Dasgupta, A., Chopra, S., 2015. Delamanid for the treatment of pulmonary multidrug-resistant tuberculosis. *Drugs Today (Barc.)* 51, 117–123.
- Vasilyev, D., Merrill, T., Iwanow, A., Dunlop, J., Bowlby, M., 2006. A novel method for patch-clamp automation. *Pflugers Arch.* 452, 240–247.
- Vazquez, M.J., Ashman, S., Ramon, F., Calvo, D., Bardera, A., Martin, J.J., Rudiger, M., Tew, D., Dominguez, J.M., 2006. Utilization of substrate-induced quenching for screening targets promoting NADH and NADPH consumption. *J. Biomol. Screen.* 11, 75–81.
- Vilcheze, C., Jacobs Jr., W.R., 2007. The mechanism of isoniazid killing: clarity through the scope of genetics. *Annu. Rev. Microbiol.* 61, 35–50.
- Vilcheze, C., Baughn, A.D., Tufariello, J., Leung, L.W., Kuo, M., Basler, C.F., Alland, D., Sacchettini, J.C., Freundlich, J.S., Jacobs Jr., W.R., 2011. Novel inhibitors of InhA efficiently kill *Mycobacterium tuberculosis* under aerobic and anaerobic conditions. *Antimicrob. Agents Chemother.* 55, 3889–3898.
- Wakamoto, Y., Dhar, N., Chait, R., Schneider, K., Signorino-Gelo, F., Leibler, S., McKinney, J.D., 2013. Dynamic persistence of antibiotic-stressed mycobacteria. *Science* 339, 91–95.
- Wikler, M.A., 2009. Methods for dilution antimicrobial susceptibility tests for bacteria that grow aerobically: approved standard. National Committee for Clinical Laboratory Standards, 2009.
- Zhang, Y., Yew, W.W., 2009. Mechanisms of drug resistance in *Mycobacterium tuberculosis*. *Int. J. Tuberc. Lung Dis.* 13, 1320–1330.
- Zhang, J.H., Chung, T.D., Oldenburg, K.R., 1999. A simple statistical parameter for use in evaluation and validation of high throughput screening assays. *J. Biomol. Screen.* 4, 67–73.
- Zumla, A., George, A., Sharma, V., Herbert, N., Baroness Masham of Ilton, 2013. WHO's 2013 global report on tuberculosis: successes, threats, and opportunities. *Lancet* 382, 1765–1767.